STEM CELLS AND DEVELOPMENT
Volume 22, Number 9, 2013

DOI: 10.1089/scd.2012.0486

# Umbilical Cord Blood-Derived Mesenchymal Stem Cells Inhibit, But Adipose Tissue-Derived Mesenchymal Stem Cells Promote, Glioblastoma Multiforme Proliferation

Keiko Akimoto,[1] Kenichi Kimura,[1] Masumi Nagano,[1] Shingo Takano,[2] Georgina To'a Salazar,[1] Toshiharu Yamashita,[1] and Osamu Ohneda[1]

Mesenchymal stem cells (MSCs) possess self-renewal and multipotential differentiation abilities, and they are thought to be one of the most reliable stem cell sources for a variety of cell therapies. Recently, cell therapy using MSCs has been studied as a novel therapeutic approach for cancers that show refractory progress and poor prognosis. MSCs from different tissues have different properties. However, the effect of different MSC properties on their application in anticancer therapies has not been thoroughly investigated. In this study, to characterize the anticancer therapeutic application of MSCs from different sources, we established two different kinds of human MSCs: umbilical cord blood-derived MSCs (UCB-MSCs) and adipose-tissue-derived MSCs (AT-MSCs). We used these MSCs in a coculture assay with primary glioblastoma multiforme (GBM) cells to analyze how MSCs from different sources can inhibit GBM growth. We found that UCB-MSCs inhibited GBM growth and caused apoptosis, but AT-MSCs promoted GBM growth. Terminal deoxynucleotidyl transferase-mediated biotinylated UTP nick-end labeling assay clearly demonstrated that UCB-MSCs promoted apoptosis of GBM via tumor necrosis factor-related apoptosis-inducing ligand (TRAIL). TRAIL was expressed more highly by UCB-MSCs than by AT-MSCs. Higher mRNA expression levels of angiogenic factors (vascular endothelial growth factor, angiopoietin 1, platelet-derived growth factor, and insulin-like growth factor) and stromal-derived factor-1 (SDF-1/CXCL12) were observed in AT-MSCs, and highly vascularized tumors were developed when AT-MSCs and GBM were cotransplanted. Importantly, CXCL12 inhibited TRAIL activation of the apoptotic pathway in GBM, suggesting that AT-MSCs may support GBM development in vivo by at least two distinct mechanisms—promoting angiogenesis and inhibiting apoptosis. The opposite effects of AT-MSCs and UCB-MSCs on GBM clearly demonstrate that differences must be considered when choosing a stem cell source for safety in clinical application.

## Introduction

Mesenchymal stem cells (MSCs) isolated from a great variety of tissues have been evaluated with respect to their phenotypes, proliferation and differentiation ability, secretion of soluble factors that activate development, and homing functions [1,2]. Indeed, MSCs can be isolated from adult tissues, including bone [1], fat [3], skeletal muscle [4], synovium [5], dental pulp [6], and fetal tissues, including umbilical cord blood [7,8], placenta [9,10], amniotic membranes and fluid [11], and Wharton's jelly [12]. MSCs are adherent, self-renewing cells that have the ability to differentiate into osteoblasts, chondrocytes, and adipocytes. MSC-specific cell surface markers have yet to be determined, but MSCs are reported to be positive for cell surface markers CD105, CD73, HLA-ABC, CD29, CD44, CD71, CD90, CD106, CD120a, and CD129, and negative for CD45, CD14, CD31, and CD34 markers [1,2,13]. Although MSCs derived from different sources share many characteristic features, they differ in many aspects of gene expression profile and physiology.

In addition to recent studies describing the tissue regeneration capability of MSCs, MSCs have been identified as promising therapeutic tools for treating cancer [14–16]. Mainly, the efficacy of MSCs to deliver anticancer molecules to sites of tumors has been studied. Delivery of molecules, including interferons [14–17], interleukins [18–20], and apoptotic inducers [21,22], has been investigated. The poor immunogenicity of MSCs represents an additional advantage for cell-based cancer therapy.

Glioblastoma multiforme (GBM) are the most aggressive primary brain tumors in humans. Despite advances in neurosurgery, radiotherapy, and chemotherapy, the prognoses for most patients with GBM are very poor [23]. To minimize the loss of brain function, a certain amount of glioma mass should remain in the primary site after surgical resection.

Graduate School of Comprehensive Human Sciences, [1]Department of Regenerative Medicine, [2]Department of Neurosurgery, University of Tsukuba, Tsukuba, Japan.

Therefore, it would be useful to combine the surgical treatment with chemotherapy, radiation, and cell-based therapy [24].

A new approach for targeting brain tumor cells has been developed using stem cells to deliver therapeutic genes and products to tumor sites. For targeted delivery, neural stem cells (NSCs) have been well studied and applied [25,26]. However, isolation and use of NSCs are limited by ethics concerns, and MSCs have been proposed as an alternative type of therapeutic stem cells. On the other hand, the proposed use of MSCs in cancer therapies is controversial, because MSC promotion of tumor vascularization has been reported previously [27,28]. MSCs may promote cancer progression and the invasive tendency of tumors.

MSCs, depending on their source tissue, can be easier to harvest and expand in vitro. Bone marrow (BM)-MSCs have been used for delivery of target genes [16,17,19,20]. However, because of donor morbidity and small expansion capacity, other sources of MSCs would be of considerable use for cancer therapy [16]. Umbilical cord blood-derived MSCs (UCB-MSCs) are being evaluated for use in cell therapy. UCB-MSCs are in a primitive stage, provoke less immune response, and possess large expansion capacity [2,7,8]. Of note, UCB-MSCs can be harvested without the risk to the donor. However, the frequency of UCB-MSCs is extremely low [7]. Adipose tissue-derived MSCs (AT-MSCs) might be a useful alternative source for therapeutic stem cells due to ease of isolation and extensive self-renewal capacity. In addition, AT-MSCs can be cultured for several months with low levels of senescence, retaining the potential to differentiate into various cell types [2].

Several kinds of GBM cell lines have been established and characterized, with varying expression of tumor-associated cytokines and receptors [29,30]. Here, instead of GBM cell lines, we isolated primary GBM cells and used MSC coculture and cotransplantation assays to analyze characteristics important for clinical application. We demonstrate that UCB-MSCs inhibit GBM proliferative activity, whereas AT-MSCs support GBM proliferation. We further show that among UCB-MSCs, AT-MSCs, and BM-MSCs, UCB-MSCs express the lowest level of CXCL12. Of note, the expression of tumor necrosis factor-related apoptosis-inducing ligand (TRAIL) in UCB-MSCs promoted apoptosis of gliomas, and the effect of TRAIL toward gliomas was inhibited by addition of exogenous CXCL12. Thus, we propose that to ensure the safety of anticancer therapy using MSCs, the characteristics of MSCs themselves are quite important and should be investigated before using an MSC-based therapy.

## Materials and Methods

### Isolation and culture of GBM and MSCs

Brain tumor samples were obtained from patients undergoing surgical resection for newly diagnosed World Health Organization (WHO-) grade IV glioma at the University of Tsukuba Hospital. Tissue sections were stained with hematoxylin and eosin (HE) to confirm the diagnosis of glioma according to the WHO criteria [31]. The research followed the tenet of the Declaration of Helsinki, and written informed consent was obtained from each eligible participant. GBM samples were minced and treated with 0.1% collagenase (Nitta Gelatin, Osaka, Japan)/20% fetal bovine serum (FBS) (Hyclone, South Logan, UT)/PBS solution at 37°C for 1 h. Cells were cultured in Dulbecco's modified Eagle's medium (DMEM)-high glucose (Invitrogen, Carlsbad, CA) with 10% FBS (Hyclone), 0.1 mM nonessential amino acid (Invitrogen), 2 mg/mL L-glutamine (Invitrogen), 0.1 mM 2-mercaptoethanol (Invitrogen), and 0.1% (v/v) penicillin–streptomycin (100 U/mL penicillin, 0.1 mg/mL streptomycin; Invitrogen) in a 25-$cm^2$ tissue culture-treated flask (Sumitomo-Bakelite, Osaka, Japan) at 37°C in 5% $CO_2$ and in a humidified atmosphere. Adherent cells were treated with trypsin (Invitrogen) and passed through a cell strainer (Falcon 3078; pore size 100 μm; BD Bioscience, San Jose, CA). Then, cells were purified for CD31−/CD45− cells using FACSVantageSE (BD Biosciences, San Jose, CA) to remove endothelial and hematopoietic cells. Surgical samples derived from 15 patients were analyzed, and five samples were successfully maintained in the culture. Pathological analysis showed that three samples were GBM (two samples were ependymoma), and two primary GBM cells (named as GBM#1 and GBM#12) were selected for further analysis because of high growth activity.

MSCs were isolated from umbilical cord blood and adipose tissues as described previously [7]. Briefly, human full-term UCB samples were collected from umbilical cord veins, and adipose tissue was collected from healthy donors with permission from the local ethics authorities at the University of Tsukuba. The clusters formed in the flask from UCB were analyzed by the uptake of phycoerythrin (PE)-conjugated low-density lipoprotein from the human plasma-acetylated DiI complex (DiI-Ac-LDL; Molecular Probes-Invitrogen, Eugene, OR). DiI-Ac-LDL uptake-negative, CD31-negative, and CD45-negative fractions were sorted using FACSVantageSE (BD Bioscience). After adherent cells from adipose tissue were expanded, they were purified for CD31−/CD45− cells using FACSVantageSE to remove endothelial and hematopoietic cells. The culture medium for UCB-MSCs and AT-MSCs consisted of Iscove's modified Dulbecco's medium (IMDM) (Invitrogen) with 10% FBS (Hyclone), 2 mg/mL L-glutamine (Invitrogen), 10 ng/mL human basic fibroblast growth factor (b-FGF) (Peprotech, London, United Kingdom), and 0.1% (v/v) penicillin–streptomycin (100 U/mL penicillin, 0.1 mg/mL streptomycin; Invitrogen). Cells ware maintained in a 25-$cm^2$ tissue culture-treated flask at 37°C in 5% $CO_2$ and in a humidified atmosphere. All experiments were performed using at least two distinct sources of UCB and adipose tissue, and results were reproducible.

### Cell lines

The GBM cell line, U87MG, was maintained in DMEM low-glucose (Invitrogen) with 10% FBS (Hyclone) and 0.1% (v/v) penicillin–streptomycin (100 U/mL penicillin, 0.1 mg/mL streptomycin; Invitrogen) in a 25-$cm^2$ tissue culture-treated flask (Sumitomo-Bakelite).

### Animals

C57BL/6J mice were purchased from Japan SLC, Inc. (Shizuoka, Japan). Animals were treated in accordance with the National Institutes of Health guide for the Care and Use of Laboratory Animals. All experimental procedures were approved by the University of Tsukuba Institute Animal Care and Use Committee.

### shRNA

To downregulate CXCR7 expression in GBM cells, we used the shRNA MISSION lentiviral transduction system (NM_020311; clone: TRCN0000014512; sequence: 5′-CCGG CGCTCTCCTTCATTTACATTTCTCGAGAAATGTAAATG AA GGAGAGCGTTTTT-3′; Sigma-Aldrich, St. Louis, MO) according to the manufacturer's protocol. After infected cells were selected using puromycin, mRNA expression of the CXCR7 level was analyzed by quantitative reverse transcription-polymerase chain reaction (RT-PCR).

### Annexin V binding assay

Apoptotic cells were detected by staining using an Annexin V-PE kit (BD Biosciences, Bedford, MA) according to the manufacturer's instructions. GBM coculture with MSCs was treated with trypsin, and then cells were stained with surface markers and washed twice with PBS. Next, labeled cells were resuspended in the Annexin V-binding buffer containing PE-conjugated Annexin V and 7-amino-actinomycin (7-AAD) and incubated at room temperature for 15 min in the dark. Cells were analyzed using FACSVantageSE. The PE-negative population was defined as viable cells. The PE-positive/7-AAD-negative ($PE^+/7\text{-}AAD^-$) population was defined as early apoptotic cells. The PE-positive/7-AAD-positive ($PE^+/7\text{-}AAD^+$) population was defined as necrotic cells.

### In vitro GBM-MSC coculture assay

Green fluorescence protein (GFP)-labeled UCB-MSCs and AT-MSCs were prepared as described previously [32]. GBM cells or U87MG cells ($2\times10^4$ cells/well) were either cultured alone or cocultured with GFP-labeled UCB-MSCs or AT-MSCs ($2\times10^4$ cells/well or $4\times10^4$ cells/well) in 35-mm dishes (Sumitomo-Bakelite) for 3 or 7 days in IMDM (Invitrogen) supplemented with 10% FBS (Hyclone), 2 mg/mL L-glutamine (Invitrogen), and 0.1% (v/v) penicillin–streptomycin (100 U/mL penicillin, 0.1 mg/mL streptomycin; Invitrogen). GBM and UCB-MSCs were treated with 10 ng/mL recombinant human CXCL12 (R&D Systems, Minneapolis, MN) and/or 1 ng/mL recombinant human TRAIL (R&D Systems), respectively. The total cell number was scored by a hemocytometer under a microscope with trypan blue staining. The frequency of GFP-labeled MSCs in each sample was determined using a flow cytometer (FACScalibur; BD Biosciences, San Jose, CA). All experiments were done in triplicate.

### In vivo subcutaneous cotransplantation of GBM-MSCs

Mice were anesthetized by intraperitoneal injection of 2,2,2-tribromoethanol (200 mg/kg). Xenografts were obtained by subcutaneous injection of GBM cells ($1\times10^6$ cells) with or without MSCs ($2\times10^6$ cells) in 100 μL of growth factor-reduced Matrigel (BD Biosciences, San Jose, CA). Tumor growth was monitored daily by measuring the average tumor diameter (two perpendicular axes of the tumor were measured by a caliper). After 18 days, mice were sacrificed by cervical dislocation, and the tumor mass was excised and weighed. Immunosuppression was performed by intraperitoneal injection of cyclosporin-A (Wako, Osaka, Japan) at 20 mg/kg body weight, 2 days before the assay. The injection of cyclosporin-A was continued daily for the entire period of the assay.

### Immunohistochemistry

Tumor specimens and cotransplanted GBM-MSC mass were harvested and were fixed with 4% paraformaldehyde. Cryostat sections (5 μm) were stained using HE, anti-glial fibrillary acidic protein (GFAP, 1:2,000; Dako, Carpinteria, CA), CD31 (1:800 for primary tumor specimens, clone: JC70A, Dako; 1:200 for cotransplanted tumor specimens, clone: MEC 13.3, BD Biosciences, San Diego, CA), and Ki-67 (1:100, clone; MIB-1, Dako) antibodies. Samples were visualized by an EnVision$^+$ kit (HRP [DAB]; Dako) after staining with primary antibodies and by the Vectastain Elite ABC standard kit after staining with secondary antibodies (Vector Laboratories, Inc., Burlingame, CA).

### Terminal deoxynucleotidyl transferase-mediated biotinylated UTP nick-end labeling assay

After cotransplantation of GBM with MSCs, cryostat sections (5 μm) were stained using a terminal deoxynucleotidyl transferase-mediated biotinylated UTP nick end labeling (TUNEL) assay kit conjugated with anti-FITC HRP (TaKaRa, Ohtsu, Japan). Brown, TUNEL-positive cells of three different areas in a single section were counted.

### Growth curve

GBM cells were plated at a density of $2\times10^4$ cells per 35-mm tissue culture dish (Sumitomo-Bakelite) and cultured under normoxic conditions (20% $O_2$). The cell culture medium was changed to fresh one every 4th day. The numbers of live cells in triplicate dishes were scored using a hemocytometer at 24-h intervals for 10 days. Dead cells were excluded by the use of trypan blue staining solution (Invitrogen).

### Microscopy analysis

Cell samples were viewed with an Olympus IX71 microscope system (Olympus, Tokyo, Japan) using LCPlanFL objective lenses at 4×/0.13PhL, 10×/0.30Ph1, and 20×/0.40Ph1. Sample slides were viewed with an Olympus BX51 microscope system (Olympus) using UPlanSApo objective lenses at 4×/0.16PH, 10×/0.40PH, and 20×/0.75PH (Olympus) and mounting reagent (Muto Pure Chemicals, Tokyo, Japan). Data were acquired with the DP70 digital camera attached to the microscope and DP controller software (Olympus). Images were processed using Adobe Photoshop version 8.0 software (Adobe System, San Jose, CA).

### Quantitative PCR

Total RNA (1 μg) was reverse transcribed using a ReverTra-Plus™ kit (Toyobo, Osaka, Japan). The reaction mixtures for quantitative PCR were prepared using the POWER SYBR® Green PCR master mix (Applied Biosystems, Carlsbad, CA) and analyzed by a 7700 Sequence Detector (Applied Biosystems). Experiments were performed as triplicate, and the data were calculated using the DDCt method. The sequence of primer sets used for the PCRs is shown in Table 1.

Table 1. Primers Used for Polymerase Chain Reaction

| | | |
|---|---|---|
| *VEGF* | 5′ primer | AGATGAGCTTCCTACAGCACAAC |
| | 3′ primer | AGGACTTATACCGGGATTTCTTG |
| *CXCL12* | 5′ primer | ATGAACGCCAAGGTCGTGGTC |
| | 3′ primer | CTTGTTTAAAGCTTTCTCCAGGTACT |
| *CXCR-4* | 5′ primer | TTTTAAGACCGCATTCTCTTTACC |
| | 3′ primer | ATTCTCCTAAAGCGCAAAAACTTA |
| *CXCR-7* | 5′ primer | TAAATATATGCCAGTCTTGGCTGA |
| | 3′ primer | TTACAAAGCAGTTTTCGTTCCATA |
| *PDGFR-α* | 5′ primer | AAAGAGCTGGATATCTTTGGATTG |
| | 3′ primer | CTAGCATGGGGACATACTGTGTAG |
| *PDGFR-β* | 5′ primer | GTAAGATGGGAAAGTTAGGCTTGA |
| | 3′ primer | ACCACCTCAGTAACTCCAAGAATC |
| *IGFR* | 5′ primer | ATTTCACACGTCTTTGTTCAGTGT |
| | 3′ primer | GTTAACACTGCTGTTGTACCCAAG |
| *EGFR-WT* | 5′ primer | ACCTGCGTGAAGAAGTGTCC |
| | 3′ primer | CCGTCTTCCTCCATCTCATAGC |
| *EGFR-vIII* | 5′ primer | AAGAAAGGTAATTATGGTGGTGACA |
| | 3′ primer | CCGTCTTCCTCCATCTCATAGC |
| *TGF-α* | 5′ primer | AATGACTGCCCAGATTCCCAC |
| | 3′ primer | CACTGAATAACCCCAAGCCGAC |
| *TGF-β* | 5′ primer | AGAGCTCCGAGAAGCGGTACCTGAACCC |
| | 3′ primer | GTTGATGTCCACTTGCAGTGTGTTATCC |
| *Ang-1* | 5′ primer | CTGACTCACATAGGGTGCAGCAATCAG |
| | 3′ primer | AGGCTGGTTCCTATCTCCAGCATGGTA |
| *PDGF-α* | 5′ primer | TGGACAGAACCCAAATTCTTTATT |
| | 3′ primer | GGCTCTCAGGTATACAAAACAGGT |
| *PDGF-β* | 5′ primer | TTAGAGATGGAGTTTGCTGTTGAG |
| | 3′ primer | TGGAGGTAGAGAGATGAAAGGAAC |
| *IGF* | 5′ primer | TGTTAAACTTTGGAACACCTACCA |
| | 3′ primer | TCACTCCTAAAGACAATGTTGGAA |
| *EGF* | 5′ primer | CATTACAGAATCTCAACACATGCTAGTGGC |
| | 3′ primer | CAAGACAGTGAATCCCATCTCCTTGGTAGCC |
| *FGF2* | 5′ primer | TTCTAAATGTGTTACGGATGAG |
| | 3′ primer | TTCAGTGCCACATACCAACTGG |
| *TRAIL* | 5′ primer | CGATTTCAGGAGGAAATAAAAGAA |
| | 3′ primer | TCCATATTCTGCATCTTTAGACCA |
| *TNF-α* | 5′ primer | CCTGTGAGGAGGACGAACAT |
| | 3′ primer | AGGCCCCAGTTTGAATTCTT |
| *TNF-β* | 5′ primer | CACCGGAGCTTTCAAAGAAG |
| | 3′ primer | TGCTCTTCCTCTGTGTGTGG |
| *FasL* | 5′ primer | GGGGGCAGTGTTCAATCTTA |
| | 3′ primer | TGGAAAGAATCCCAAAGTGC |
| *DR4* | 5′ primer | ACATGCAAGAGAGAAGATTCAGG |
| | 3′ primer | TAACACCTAAGAGGAAACCTCTGG |
| *DR5* | 5′ primer | ATCTTGGCTCAGTGCAACCT |
| | 3′ primer | TGGTGAAACCCCGTCTCTAC |
| *DcR1* | 5′ primer | CCAACGCTTCCAACAATGAA |
| | 3′ primer | GGCATTGGCACCAAATTCTT |
| *DcR2* | 5′ primer | CTCAGGTGGTGGAGGAGGTC |
| | 3′ primer | GTGGCTCCTCTGGCAACTCT |
| *TNFR-α* | 5′ primer | GAGAGGCCATAGCTGTCTGG |
| | 3′ primer | GTTCCTTTGTGGCACTTGGT |
| *TNFR-β* | 5′ primer | ATTCTGGGAGGAAGCAGGTT |
| | 3′ primer | AGCCAGCCAGTCTGACATCT |
| *Fas* | 5′ primer | ATGGCCAATTCTGCCATAAG |
| | 3′ primer | TGGAAGAAAAATGGGCTTTG |
| *β-Actin* | 5′ primer | GTGCGTGACATTAAGGAGAAGCTGTGC |
| | 3′ primer | GTACTTGCGCTCAGGAGGAGCAATGAT |

VEGF, vascular endothelial growth factor; PDGF, platelet-derived growth factor; TGF, transforming growth factor; IGF, insulin-like growth factor; EGF, epidermal growth factor; FGF, fibroblast growth factor; TNF, tumor necrosis factor; Ang-1, angiopoietin 1; TRAIL, tumor necrosis factor-related apoptosis-inducing ligand.

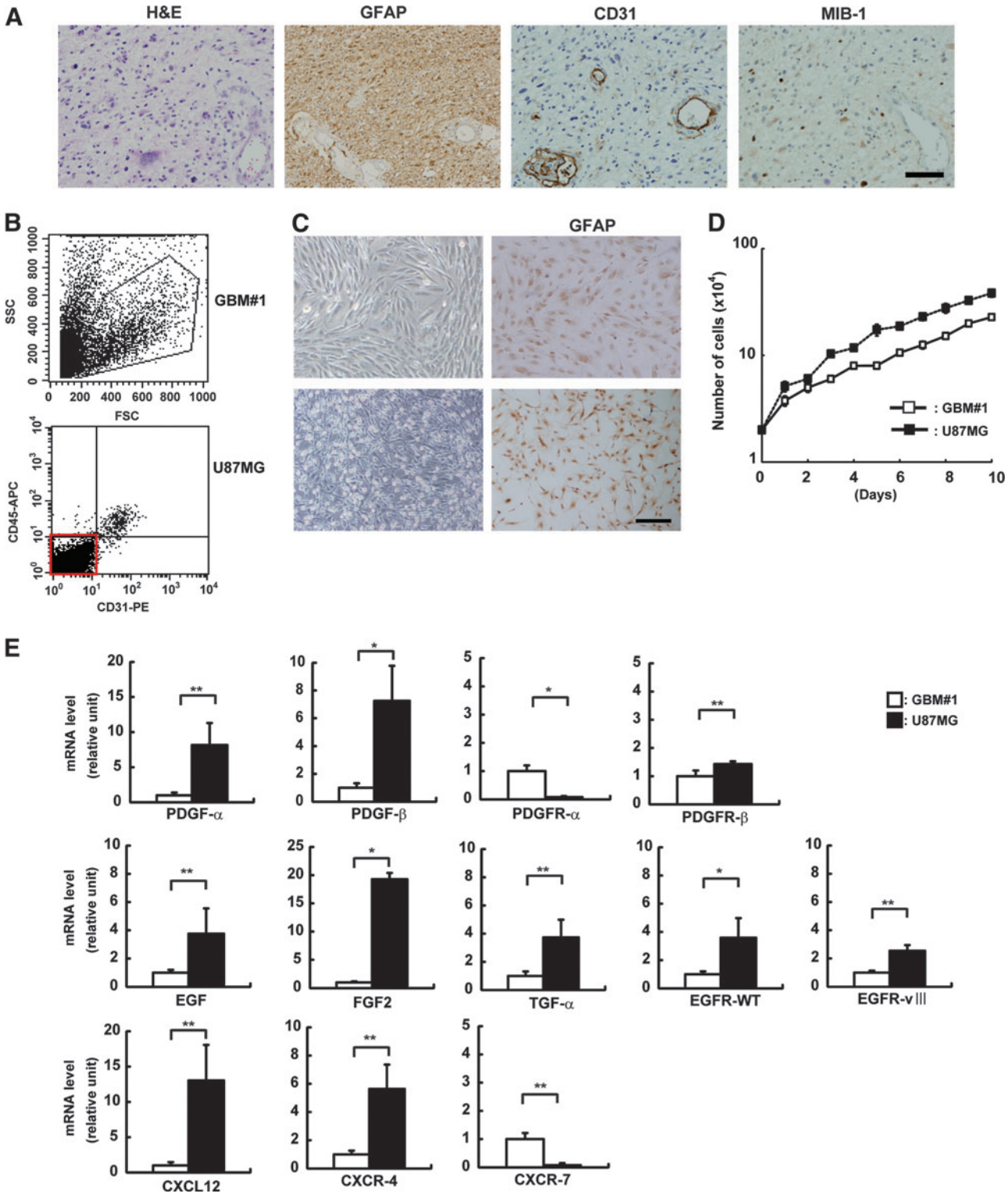


**FIG. 1.** Isolation of primary glioblastoma multiforme (GBM) cells from patients. **(A)** Histological analysis was performed for GBM tissues by immunostaining. Specimens were stained with H&E: hematoxylin–eosin staining, glial fibrillary acidic protein (GFAP): astrocyte markers, CD31: endothelial markers, and MIB-1 (Ki-67): proliferation markers. Scale bar indicates 100 μm. **(B)** Adherent cells derived from GBM tissues were purified for nonhematopoietic (CD45-negative) and nonendothelial (CD31-negative) cells by fluorescence activated cell sorting (FACS). **(C)** CD45 – /CD31 – cells were purified and expanded for further experiments. Primary GBM cells (GBM#1) and U87MG showed fibroblastic morphology and expressed GFAP by immunostaining. Scale bar indicates 100 μm. **(D)** Growth activity was measured in primary GBM#1 and U87MG cells. Cells were harvested every 24 h until cells reached at a confluent state. The average cell number in triplicate dishes was determined (mean ± SD). Note that the growth rate of U87MG (*black squares*) was faster than that of GBM#1 (*white squares*). **(E)** mRNA expression of each factor in GBM#1 and U87MG was examined by real-time polymerase chain reaction. *White bar* indicates GBM#1; *black bar*, U87MG. The mRNA expression seen in GBM#1 was normalized to a value of 1 as the standard for each factor (*$P < 0.05$; **$P < 0.01$). Color images available online at www.liebertpub.com/scd

### Enzyme-linked immunosorbent assay

Supernatants of UCB-MSCs and AT-MSCs were harvested after 2 days of culture. Each supernatant was centrifuged at 2,000 *g* for 10 min at 4°C and stored at −80°C before use. The collected each conditioned medium was analyzed with an enzyme-linked immunosorbent assay (ELISA) kit for CXCL12 (R&D Systems) and TRAIL (R&D Systems). The total protein concentration of cytosol extracts was measured with the Bio-Rad protein assay (Bio-Rad Laboratories, Hercules, CA). CXCL12 and TRAIL protein expression was measured according to the manufacturer's instructions.

### Statistical analysis

Data were statistically evaluated using the Student's *t*-test for pair-comparison analysis. Data are presented as mean ± SD.

## Results

### Characterization of primary cultured GBM cells

Tissue specimens of GBM were highly cellular and composed of fibrillary astrocytes with tumor-giant cells (Fig. 1A). Most cells were strongly positive for GFAP. Tumor vessels surrounded by CD31-positive endothelial cells were observed in the specimens. The percentage of nuclei positive for the tumor cell proliferation marker Ki-67/MIB-1 ranged from 12% to 20% (mean labeling index: 16.7% ± 3.2%).

To eliminate hematopoietic cells and endothelial cells, primary cultured adherent cells were expanded and sorted by fluorescence activated cell sorting (FACS) (Fig. 1B). Isolated CD45−/CD31− cells had fibroblastic morphology and stained positive with GFAP antibody (Fig. 1C).

The proliferative ability of primary cultured GBM cells (GBM#1) was examined. Doubling time was 84.4 h. By contrast, the doubling time of the GBM cell line, U87MG, was 68.9 h, indicating that while GBM#1 showed good proliferative ability, U87MG showed more robust proliferative potential than primary cultured GBM #1 cells (Fig. 1D).

We then examined the expression levels of genes that may affect proliferation and survival of glioma cells. Platelet-derived growth factor (PDGF)-α/β, epidermal growth factor (EGF), fibroblast growth factor 2 (FGF2), and transforming growth factor-α (TGF-α) were expressed more highly in U87MG than in GBM#1. Receptors of PDGF (PDGFR-β) and EGF (EGFR) were expressed at higher levels in U87MG, whereas PDGFR-α expression was slightly higher in GBM#1. Of note, the chemokine CXCL12 (also known as SDF-1) was expressed at a high level in U87MG as compared with GBM#1. The CXCL12 receptor CXCR4 was expressed more highly in U87MG, whereas the CXCL12 receptor CXCR7 was expressed at a higher level in GBM#1 (Fig. 1E).

### Coculture of GBM cells and MSCs in vitro

Cytotoxicity of MSCs against GBM was examined by in vitro coculture assay. At first, we examined whether UCB-derived MSCs possess cytotoxicity against GBM at different cell ratios. In this study, the number of GBM cells was scored by FACS after 3- and 7-day coculture with GFP-labeled MSCs. When GBM#1 or U87MG cells were cocultured with UCB-MSCs at a 1:1 ratio, no decrease of glioma cells was measured on days 3 and 7 (Fig. 2A). On the other hand, GBM#1 cocultured with twice as many UCB-MSCs (1:2) showed significant decrease in the number of GBM#1 on day 3 (without coculture: $4.5 \pm 0.8 \times 10^4$ cells; with coculture: $0.8 \pm 0.1 \times 10^4$ cells, $n = 3$, $P < 0.01$) and day 7 (without coculture: $11 \pm 1.4 \times 10^4$ cells; with coculture: $3.1 \pm 0.3 \times 10^4$ cells, $n = 3$, $P < 0.01$), as well as other primary GBM cells (GBM#12) (Fig. 2C; Supplementary Fig. S1B; Supplementary Data are available online at www.liebertpub.com/scd). Of note, the number of U87MG did not decrease after coculture with twice as many UCB-MSCs, indicating that primary and established GBM cells have different sensitivities to the cytotoxic effects of UCB-MSCs (Fig. 2B). Indeed, some groups have previously reported that primary glioma cells show different expression of growth and survival factors than do established glioma cell lines [30,33]. Therefore, while primary GBM cells likely better reflect the process occurring in vivo,

**FIG. 2.** Analysis of anti-GBM effects of mesenchymal stem cells (MSCs) in vitro. GBM cells ($2 \times 10^4$/well) were cocultured with MSCs ($2 \times 10^4$/well or $4 \times 10^4$/well). After culture for 3 and 7 days, the number and frequency of GBM cells and green fluorescence protein (GFP)-labeled MSCs were measured by a hemocytometer and FACS. **(A)** U87MG and GBM#1 were cocultured with umbilical cord blood-derived MSCs (UCB-MSCs) at a ratio of 1:1. The *left panel* represents the number of U87MG and the *right panel* represents the number of GBM#1 in each time point. *White bar*: number of GBM alone w/o coculture; *black bar*: number of GBM cocultured with UCB-MSCs (**$P < 0.01$). **(B)** U87MG were cocultured with UCB-MSCs at a ratio of 1:2. The *left panel* represents coculture of GFP-labeled UCB-MSCs with U87MG under fluorescence microscopy (*top*) and merged picture (*bottom*). Scale bar indicates 100 μm. The *right panel* represents the number of U87MG cells (*top graph*) cocultured with (*black bar*) or w/o GFP-labeled UCB-MSCs (*white bar*) and the number of UCB-MSCs (*bottom graph*) cocultured with (*black bar*) or w/o U87MG (*white bar*) (**$P < 0.01$). **(C)** GBM#1 was cocultured with UCB-MSCs at a ratio 1:2. The *left panel* represents coculture of GFP-labeled UCB-MSCs with GBM#1 under fluorescence microscopy (*top*) and merged picture (*bottom*). Scale bar indicates 100 μm. The *right panel* represents number of GBM#1 cells (*top graph*) cocultured with (*black bar*) or w/o GFP-labeled UCB-MSCs (*white bar*) and the number of UCB-MSCs (*bottom graph*) cocultured with (*black bar*) or w/o GBM#1 (*white bar*) (*$P < 0.05$; **$P < 0.01$). **(D)** GBM#1 was cocultured with adipose-tissue-derived MSCs (AT-MSCs) at a ratio 1:2. The *left panel* represents coculture of GFP-labeled AT-MSCs with GBM#1 under fluorescence microscopy (*top*) and merged picture (*bottom*). Scale bar indicates 100 μm. The *right panel* represents number of GBM#1 cells (*top graph*) cocultured with (*black bar*) or w/o GFP-labeled AT-MSCs (*white bar*) and the number of UCB-MSCs (*bottom graph*) cocultured with (*black bar*) or w/o GBM#1 (*white bar*) (*$P < 0.05$; **$P < 0.01$). **(E)** The effect of a conditioned medium of UCB-MSCs (*left panel*) and AT-MSCs (*right panel*) was analyzed. GBM#1 cells ($2 \times 10^4$ cells) were cultured w/o (*white bar*) or with 20% condition medium (CM) from each MSC (*black bar*). Note that CM derived from UCB-MSCs did not affect GBM growth (*left panel*), whereas CM derived from AT-MSCs promote GBM growth significantly on days 3 and 7 (**$P < 0.01$).

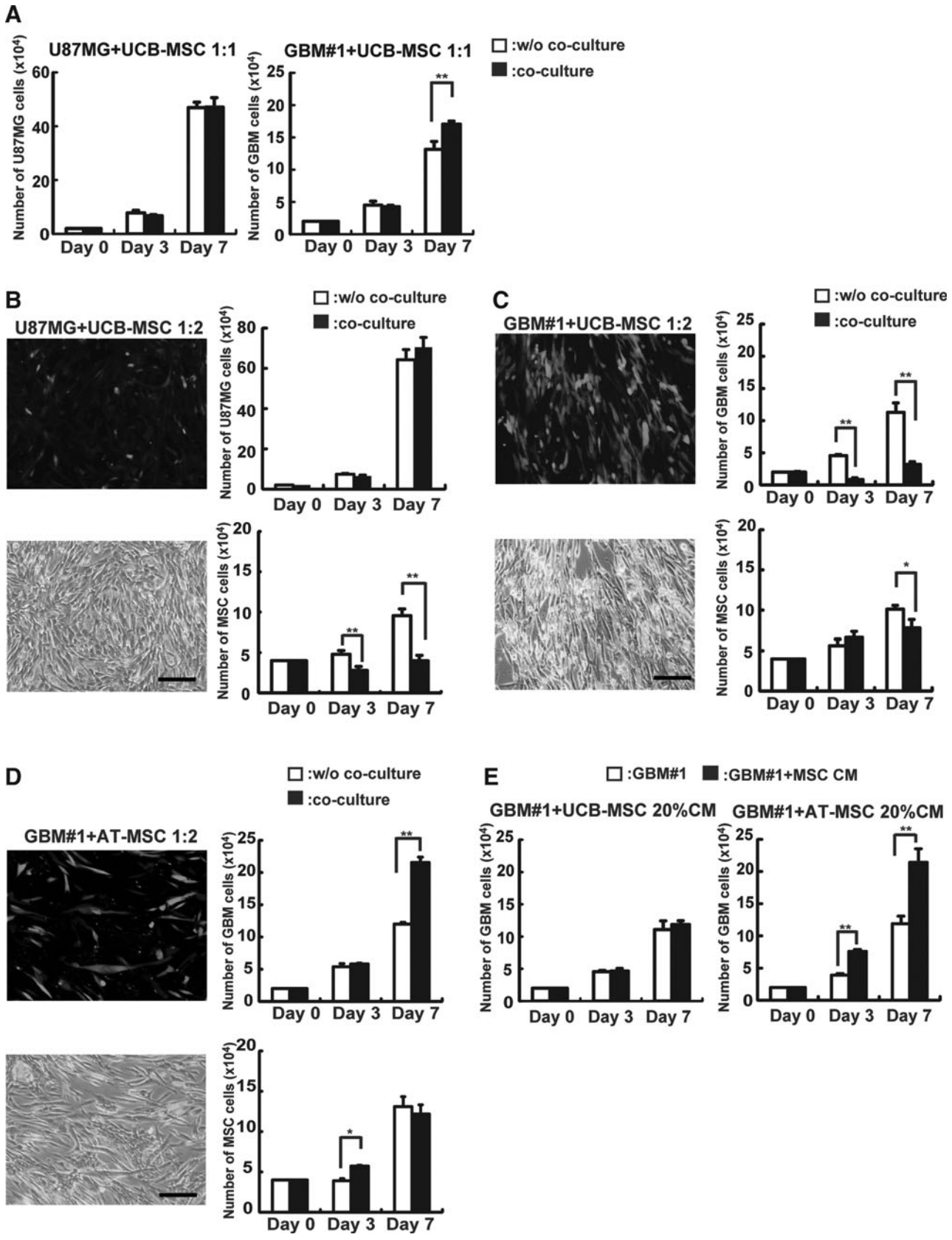
A
U87MG+UCB-MSC 1:1
GBM#1+UCB-MSC 1:1
:w/o co-culture
:co-culture
Number of U87MG cells (x10⁴)
Number of GBM cells (x10⁴)
Day 0 Day 3 Day 7
B
U87MG+UCB-MSC 1:2
Number of MSC cells (x10⁴)
C
GBM#1+UCB-MSC 1:2
D
GBM#1+AT-MSC 1:2
E
:GBM#1
:GBM#1+MSC CM
GBM#1+UCB-MSC 20%CM
GBM#1+AT-MSC 20%CM

precise biological analyses are required to assess the ability of cytotoxicity of MSCs against GBM.

We then examined whether MSCs derived from another tissue possess a similar cytotoxicity against GBM; AT-MSCs were utilized for coculture assay. After coculture with AT-MSCs for 3 days, the number of GBM#1 did not decrease (without coculture: $5.3\pm0.4\times10^4$ cells; with coculture: $5.7\pm0.1\times10^4$ cells, $n=3$, $P>0.05$), whereas the number of GBM#1 significantly increased after coculture with AT-MSCs for 7 days (without coculture: $12\pm0.2\times10^4$ cells; with coculture: $21\pm0.8\times10^4$ cells, $n=3$, $P<0.01$) (Fig. 2D). The number of AT-MSCs after 3 days' coculture with GBM#1 increased slightly (without coculture: $3.9\pm0.2\times10^4$ cells; with coculture: $5.7\pm0.1\times10^4$ cells, $n=3$, $P<0.05$), and 7-day coculture with GBM#1 was not correlated with a significant difference in the number of AT-MSCs (without coculture: $1.3\pm0.1\times10^4$ cells; with coculture: $1.2\pm0.1\times10^4$ cells, $n=3$, $P>0.05$) (Fig. 2D). In addition, after GBM#12 was cocultured with AT-MSCs for 3 days, the number of GBM#12 did not decrease (without coculture: $4.1\pm0.7\times10^4$ cells; with coculture: $4.2\pm0.2\times10^4$ cells, $n=3$, $P>0.05$), whereas the number of GBM#12 significantly increased after coculture with AT-MSCs for 7 days (without coculture: $13\pm0.9\times10^4$ cells; with coculture: $17\pm1.4\times10^4$ cells, $n=3$, $P<0.05$) (Supplementary Fig. S1C). These results indicate that the effectiveness of cytotoxicity against GBM differs among MSCs derived from different tissues. We then examined whether secreted factors in supernatant of MSCs were responsible for the cytotoxic effect. The number of GBM#1 was not significantly different in the absence or presence of a conditioned medium of UCB-MSCs (day 3: without conditioned medium, $4.5\pm0.1\times10^4$ cells; with conditioned medium, $4.6\pm0.4\times10^4$ cells; and day 7: without conditioned medium, $11\pm1.0\times10^4$ cells; with conditioned medium, $11\pm0.5\times10^4$ cells; $n=3$, $P>0.05$) (Fig. 2E). Of note, the number of GBM#1 increased on day 3 (without conditioned medium: $3.9\pm0.2\times10^4$ cells; with conditioned medium: $7.6\pm0.2\times10^4$ cells, $n=3$, $P<0.01$) and day 7 (without conditioned medium: $11\pm1.1\times10^4$ cells; with conditioned medium: $21\pm2.1\times10^4$ cells, $n=3$, $P<0.01$) in the presence of a conditioned medium from AT-MSCs, indicating that AT-MSCs may secrete some factors that support proliferation of GBM#1 (Fig. 2E).

### *Expression of growth factor and chemokine mRNA in UCB-MSCs and AT-MSCs*

To investigate the effect of MSCs on GBM#1 proliferation in vitro, mRNA expression of growth factors or chemokines was examined in UCB-MSCs and compared with those of AT-MSCs (Fig. 3). Platelet-derived growth factor-α (PDGF-α), PDGF-β, and insulin-like growth factor (IGF) were more highly expressed in AT-MSCs than in UCB-MSCs (PDGF-α: 42-fold increase; PDGF-β: 9.5-fold increase; IGF: 9-fold increase), and EGF was slightly more highly expressed in UCB-MSCs than AT-MSCs (EGF: 6-fold increase). TGF-β and FGF2 mRNAs were expressed in UCB-MSCs and AT-MSCs at similar levels. Chemokine CXCL-12 was expressed at a higher level in AT-MSCs than in UCB-MSCs (CXCL-12: 112-fold increase). We then examined the expression of angiogenic factors in UCB-MSCs and AT-MSCs. Vascular endothelial growth factor (VEGF) and angiopoietin 1 (Ang-1) were more highly expressed in AT-MSCs than in UCB-MSCs (VEGF: 5-fold increase; Ang-1: 4.9-fold increase) (Fig. 3A).

### *Analysis of CXCL12 effect on GBM-MSC coculture assay*

The time course analyses of the apoptotic cell frequency demonstrated that the highest apoptotic cell frequency occurred on day 3 of coculture of GBM#1 with UCB-MSCs (GBM#1: $2.1\%\pm1.1\%$; UCB mixture: $20.4\%\pm3.9\%$, $n=3$, $P<0.01$). The frequency of apoptotic cells gradually decreased on days 5 and 7 of coculture of GBM#1 with UCB-MSCs (Fig. 3B, C). As shown in Fig. 3A, CXCL12 was significantly more highly expressed in AT-MSCs than in UCB-MSCs. Therefore, we hypothesized that CXCL12 might have an antiapoptotic role in coculture of GBM#1 with AT-MSCs. CXCL12 was added to the coculture of GBM#1 and UCB-MSCs, and the frequency of apoptotic cells was analyzed. The frequency of apoptotic cells in GBM#1 and UCB-MSC coculture greatly decreased in the presence of CXCL12. The magnitude of decrease was similar to that of GBM#1 alone on days 3 and 5 (day 3: without CXCL12: $20.4\%\pm3.9\%$, with CXCL12: $2.0\%\pm0.3\%$; day 5: without CXCL12: $11\%\pm2.4\%$, with CXCL12: $3.8\%\pm1.2\%$, $n=3$, $P<0.01$). This result suggests that CXCL12 and its receptor are associated with the antiapoptotic effect observed in coculture of GBM and MSCs (Fig. 3B, C). Indeed, the number of GBM cells reached a level similar to that of GBM#1 alone or GBM#1 in the presence of CXCL12 on days 3 and 7 after coculture with UCB-MSCs (day 3: without CXCL12: $4.5\pm0.1\times10^4$ cells, with CXCL12: $4.6\pm0.4\times10^4$ cells; day 7: without CXCL12: $11\pm1.0\times10^4$ cells, with CXCL12: $11\pm0.5\times10^4$ cells, $n=3$, $P>0.05$). These results indicate that CXCL12 acts effectively as an antiapoptotic factor in GBM development in vitro (Fig. 3D).

### *Cotransplantation assay of GBM and MSCs in vivo*

To investigate the cytotoxic effect of MSCs on GBM#1 in vivo, GBM#1 and MSCs were mixed with Matrigel and transplanted subcutaneously into the back of mice. Cyclosporin-A used in this study did not show tumor growth suppression in the xenotransplanted mice (Supplementary Fig. S2). Tumor development was analyzed on day 18 after transplantation. When the GBM#1 and UCB-MSC mixture was transplanted into mice, the tumor weight significantly decreased compared to that derived from GBM#1 alone (GBM#1 alone: $21.3\pm1.8$ mg; GBM#1 + UCB-MSCs: $11.3\pm3.0$ mg, $n=5$, $P<0.01$). On the contrary, cotransplantation of GBM#1 and AT-MSCs generated an increase in the tumor weight compared to the transplantation of GBM#1 alone or cotransplantation of GBM#1 and UCB-MSCs (GBM#1 alone: $21.3\pm1.8$ mg; GBM#1 + AT-MSCs: $36.0\pm7.8$ mg, $n=5$, $P<0.01$) (Fig. 4A). Histological analyses revealed broad expansion of GFAP positive-stained cells in the transplantation of GBM#1 alone or transplantation of GBM#1 with AT-MSCs. A small number of weakly stained GFAP-positive cells was observed in the cotransplantation of GBM#1 and UCB-MSCs (Fig. 4B, middle panel). A higher number of CD31-positive tumor endothelial cell (EC) was observed in the transplantation of GBM#1 and AT-MSCs compared to the transplantation of GBM#1 alone or transplantation of GBM#1 with UCB-MSCs (GBM#1 alone: $49.0\pm21$ numbers/field; GBM#1 + UCB-MSCs: $11.6\pm2.0$ numbers/field; GBM#1 + AT-MSCs: $104\pm26$ numbers/field, $n=5$; GBM#1 alone vs. GBM#1 + UCB-MSCs, $P<0.01$; GBM#1 +

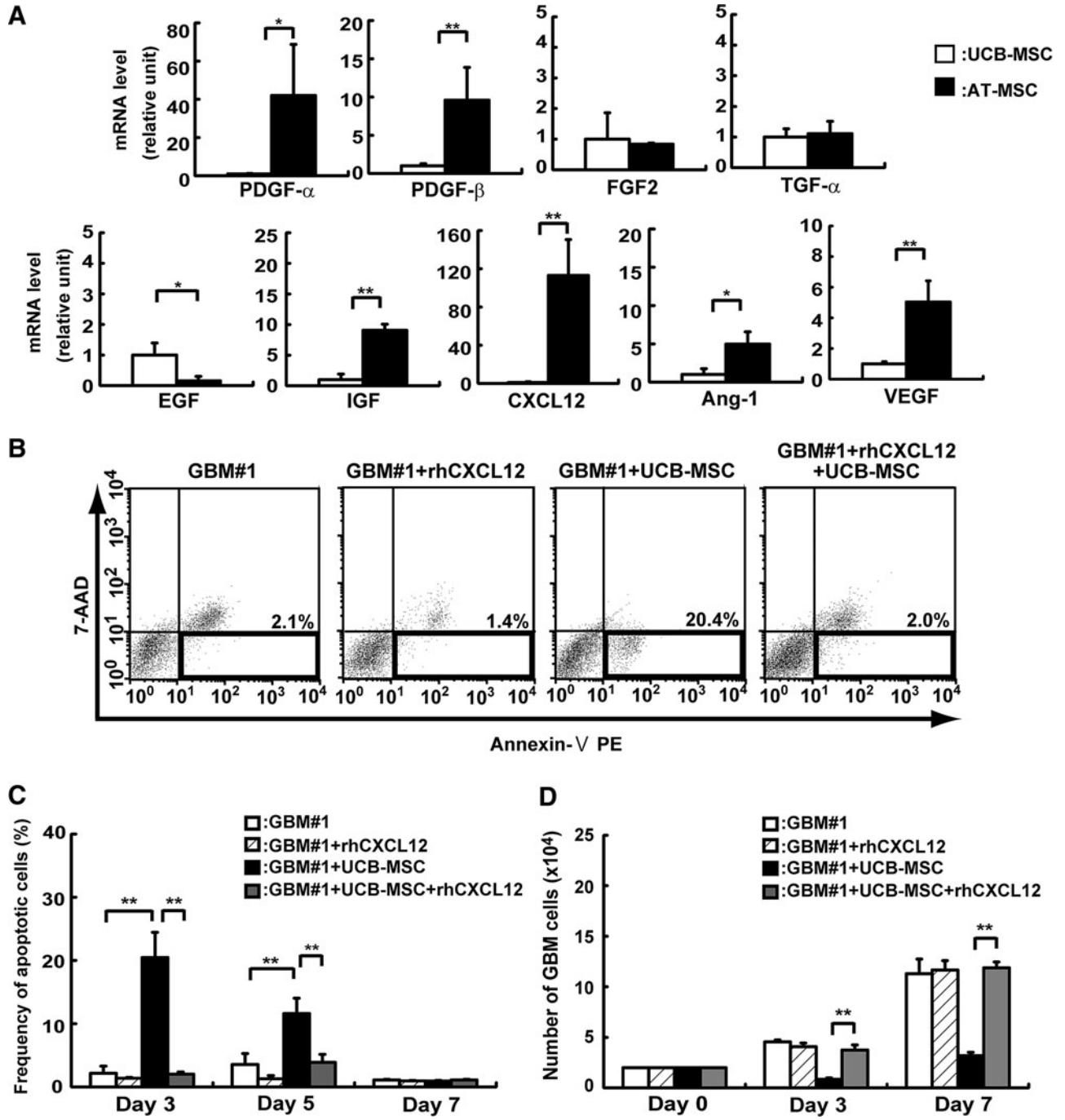


**FIG. 3.** Analysis of how MSCs affect GBM#1 survival. **(A)** Expression of growth, angiogenic, and survival factors was analyzed in UCB-MSCs and AT-MSCs by real-time PCR. The expression of factors in UCB-MSCs was normalized to a value of 1 as the standard for each factor. *White bar*: UCB-MSCs; *black bar*: AT-MSCs (*$P < 0.05$; **$P < 0.01$). **(B)** The effect of CXCL12 on GBM#1 was analyzed by FACS. Expression of Annexin V and 7-amino-actinomycin (7-AAD) was determined in the presence or absence of CXCL12. Lower right areas in each (surrounded by *bold line*) was measured as apoptotic cells according to the manufacturer's instruction. **(C)** The frequency of 7-AAD/Annexin $V^+$ cells was measured as apoptotic cells by FACS. *White bar*: GBM#1 alone; *hatched-line bar*: GBM#1 with recombinant CXCL12; *black bar*: GBM#1 + UCB-MSCs; *gray bar*: GBM#1 + UCB-MSCs with recombinant CXCL12 (**$P < 0.01$). Note that frequency of apoptotic cells after coculture of GBM#1 with UCB-MSCs greatly decreased in the presence of CXCL12. **(D)** Number of GBM#1 cells after coculture with UCB-MSCs was analyzed with or w/o CXCL12. *White bar*: GBM#1 alone; *hatched-line bar*; GBM#1 with recombinant CXCL12; *black bar*: GBM#1 + UCB-MSCs; *gray bar*: GBM#1 + UCB-MSCs with recombinant CXCL12 (**$P < 0.01$). Note that the number of apoptotic cells after coculture of GBM#1 with UCB-MSCs greatly increased in the presence of CXCL12 at the level of GBM#1 alone.

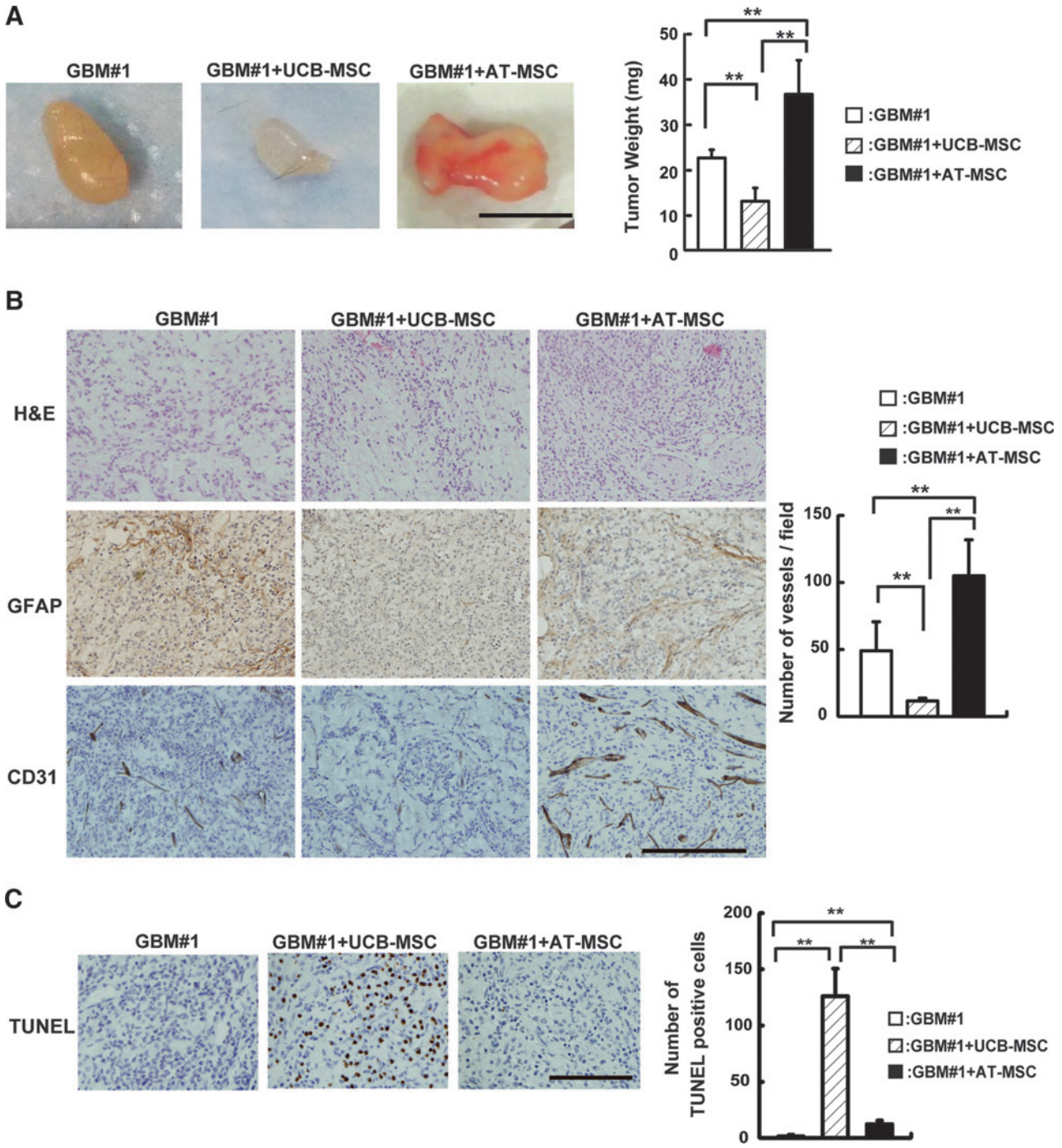


**FIG. 4.** Analysis of anti-GBM effects of MSCs in vivo. **(A)** GBM#1 ($1\times10^6$ cells) and UCB-MSCs or AT-MSCs ($2\times10^6$ cells) in 100 μL of Matrigel was inoculated subcutaneously into the mouse back skin. After 18 days post-transplantation, tumors were harvested, and tumor weights were measured (*right graph*). *White bar*: GBM#1 alone; *hatched-line bar*: GBM#1 + UCB-MSCs; *black bar*: GBM#1 + AT-MSCs (**$P<0.01$). Scale bar indicates 1 mm. **(B)** Histological analysis of transplanted tumors was performed staining with H&E (*top panel*), GFAP (*middle panel*), and CD31 (*bottom panel*) antibodies. Sectioned sample from GBM#1 alone (*left*), GBM + UCB-MSCs (*middle*), and GBM + AT-MSCs (*right*) was analyzed for morphology of GBM and angiogenesis. The number of CD31-positive cells was scored (*right graph*). *White bar*: GBM#1 alone; *hatched-line bar*: GBM#1 + UCB-MSCs; *black bar*: GBM#1 + AT-MSCs (**$P<0.01$). Scale bar indicates 200 μm. Note that the number of vessels increased when GBM#1 was transplanted with AT-MSCs. **(C)** Terminal deoxynucleotidyl transferase-mediated biotinylated UTP nick-end labeling (TUNEL) assay was performed in GBM#1-derived tumors. GBM#1 alone (*left*), GBM#1 + UCB-MSCs (*middle*), and GBM#1 + AT-MSCs (*right*). The number of TUNEL-positive cells was measured (*right graph*). *White bar*: GBM#1 alone; *hatched-line bar*: GBM#1 + UCB-MSCs; *black bar*: GBM#1 + AT-MSCs. Scale bar indicates 200 μm (**$P<0.01$). Color images available online at www.liebertpub.com/scd

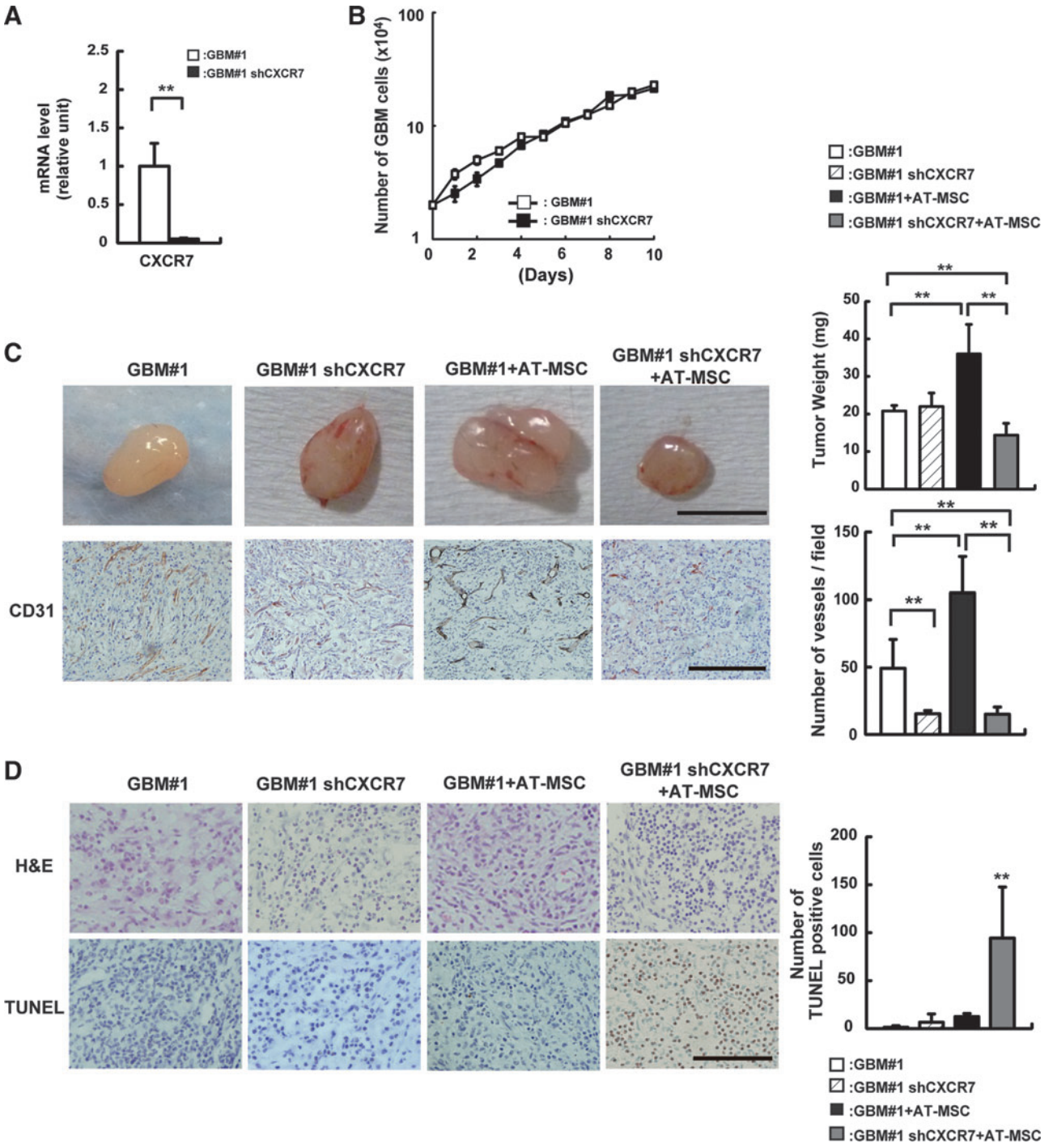


**FIG. 5.** Analysis of a role of CXCR7 in GBM#1. **(A)** *CXCR7* mRNA expression was analyzed in GBM#1 (*white bar*) and shCXCR7 GBM#1 (*black bar*). $^{**}P < 0.01$. **(B)** Growth activity was analyzed in GBM#1 (*white square*) and shCXCR7 GBM#1 (*black square*). Cells were harvested every 24 h until cells reached at a confluent state. **(C)** GBM#1 ($1 \times 10^6$ cells) and shCXCR7 GBM#1 ($1 \times 10^6$ cells) with or w/o AT-MSCs ($2 \times 10^6$ cells) in 100 mL of Matrigel was inoculated subcutaneously into the mouse back skin. At 18 days post-transplantation, tumors were harvested, and the tumor weight was measured (*right graph*). *White bar*: GBM#1 alone; *hatched-line bar*: GBM#1 shCXCR7; *black bar*: GBM#1 + AT-MSCs; *gray bar*: GBM#1 shCXCR7 + AT-MSCs ($^{**}P < 0.01$). Scale bar indicates 1 mm. **(D)** TUNEL assay was performed in GBM#1- or shCXCR7 GBM#1-derived tumors with or w/o AT-MSCs. GBM#1 alone (*left*); shCXCR7 GBM#1 alone (*second from the left*); GBM#1 + AT-MSCs (*second from the right*); GBM#1 shCXCR7 + AT-MSCs (*right*). The number of TUNEL-positive cells was measured in each tumor (*right graph*). *White bar*: GBM#1 alone; *hatched-line bar*: GBM#1 shCXCR7; *black bar*: GBM#1 + AT-MSCs; *gray bar*: GBM#1 shCXCR7 + AT-MSCs ($^{**}P < 0.01$). Scale bar indicates 200 μm. Note that the highest number of TUNEL-positive cells was observed in tumors derived from shCXCR7 + AT-MSCs. Color images available online at www.liebertpub.com/scd

UCB-MSCs vs. GBM#1 + AT-MSCs, $P < 0.01$; GBM#1 alone vs. GBM#1 + AT-MSCs, $P < 0.01$) (Fig. 4B, bottom panel and right graph).

To clarify the mechanism of cytotoxic effect of UCB-MSCs against GBM, the number of apoptotic cells was evaluated by the TUNEL assay in each tumor after transplantation. The number of TUNEL-positive cells was the highest in the cotransplantation of GBM#1 and UCB-MSCs among the harvested tumors (GBM#1 alone: $1.3 \pm 1.5$ cells/field; GBM#1 + UCB-MSCs: $126 \pm 24$ cells/field, $n = 3$, $P < 0.01$) (Fig. 4C), suggesting that a decreased number of GBM was caused by apoptosis after cotransplantation with UCB-MSCs.

### *Effect of GBM proliferation on CXCR7*

As shown in Fig. 1E, CXCL12 receptor CXCR7 was more highly expressed in GBM#1 than in U87MG. To investigate how the CXCL12/CXCR7 pathway is involved in the cytotoxicity observed in the coculture assay, expression of CXCR7 was impaired in GBM#1 using shRNA (Fig. 5A).

At first, we examined how CXCR7 is involved in the proliferation of GBM#1, and the cell doubling time was examined between GBM#1 alone and GBM#1 shCXCR7. We could not find a significant difference between them (doubling time; GBM#1: $84.4 \pm 8.4$ h; shCXCR7 GBM#1: $70.4 \pm 6.1$ h, $n = 3$, $P > 0.05$) (Fig. 5B), indicating that the CXCL12/CXCR7 axis is not associated with the proliferation of GBM#1, as previously reported [34].

In vivo transplantation analyses clearly demonstrated that shCXCR7 GBM#1 alone did not show any reduction of tumor size compared to GBM#1 alone (GBM#1: $20.5 \pm 1.4$ mg; shCXCR7 GBM#1: $22 \pm 3.6$ mg, $n = 5$, $P > 0.05$), whereas coculture of shCXCR7 GBM#1 with AT-MSCs clearly demonstrated the reduction of tumor weight compared to those of GBM#1 and AT-MSC coculture (GBM#1 + AT-MSCs: $36.0 \pm 7.8$ mg; shCXCR7 GBM#1 + AT-MSCs: $14.3 \pm 3.1$ mg, $n = 5$, $P < 0.01$) (Fig. 5C, top panel and graph). Histological analysis clearly revealed that CD31-positive cells were highly observed in GBM#1 coculture with AT-MSCs (GBM#1: $49 \pm 21.5$ vessels/field; GBM#1 + AT-MSCs: $104 \pm 26.9$ vessels/field, $n = 3$, $P < 0.01$). Interestingly, interference with the CXCR7 expression in GBM#1 showed a less number of vessels even coculture with AT-MSCs (GBM#1 shCXCR7 + AT-MSCs: $15.0 \pm 5.3$ vessels/field; GBM#1 + AT-MSCs: $104 \pm 26.9$ vessels/field, $n = 3$, $P < 0.01$) (Fig. 5C, bottom panel and graph). Consistent with these data, the frequency of apoptotic cells and TUNEL-positive cells increased in coculture of shCXCR7 GBM#1 and AT-MSCs compared to that of GBM#1 and AT-MSC coculture (shCXCR7: $94.3 \pm 53.1$ cells/field; GBM: $12.3 \pm 3.2$ cells/field, $n = 5$, $P < 0.01$) (Fig. 5D). Moreover, the frequency of apoptotic cells slightly increased in shCXCR7 GBM#1 alone compared to GBM#1 alone, even though the cell proliferation activity was not significantly different between GBM#1 and shCXCR7 GBM#1 (Fig. 5B).

### *TRAIL secreted from UCB-MSCs affected GBM apoptosis*

TRAIL-based cancer therapies against glioma have been previously analyzed [21,22]. We investigated expression of TRAIL and tumor necrosis factor (TNF) in MSCs and TRAIL receptors in GBM. Expression of TRAIL, TNF-α, and TNF-β was higher in UCB-MSCs than in AT-MSCs (TRAIL: 45-fold; TNF-α: 5-fold; TNF-β: 10-fold increase), whereas FasL was expressed at a similar extent in UCB-MSCs and AT-MSCs (Fig. 6A).

While mRNA expression of TRAIL receptors possessing a death domain (DR4 and DR5) was higher in U87MG compared to GBM#1 (DR4: 9-fold; DR5: 7-fold increase), mRNA expression of TRAIL decoy receptors (DcR1 and DcR2) was also detected at a higher level in U87MG than in GBM#1 (DcR1: 7-fold; DcR2: 6-fold increase), suggesting that high expression of DcR1 blocks DR5 functions in TRAIL-induced apoptosis, which might be caused in UCB-MSC and U87MG coculture (Fig. 6B).

Collectively, these data suggest that TRAIL expressed in UCB-MSCs act effectively on TRAIL receptors of GBM#1, but not on those of U87MG.

### *CXCL12 inhibits TRAIL pathway on GBM*

From previous results, we hypothesized that TRAIL pathway might have an important role in coculture of GBM#1 and UCB-MSCs and have an apoptotic effect. Thus, we added recombinant TRAIL exogenously to GBM#1 culture and examined the number of live and dead cells. GBM#1 in the presence of recombinant TRAIL showed a significantly decreased number of live GBM#1 on day 3 (GBM alone: $3.4 \pm 0.2 \times 10^4$ cells; with TRAIL: $0.8 \pm 0.2 \times 10^4$ cells, $n = 3$, $P < 0.01$) and day 7 (GBM alone: $10 \pm 0.3 \times 10^4$ cells; with TRAIL: $2.6 \pm 0.1 \times 10^4$ cells, $n = 3$, $P < 0.01$) (Fig. 6C, left panel). On the other hand, the number of dead GBM#1 increased on day 7 (GBM alone: $1.0 \pm 0.1 \times 10^4$ cells; with TRAIL: $1.6 \pm 0.1 \times 10^4$ cells, $n = 3$, $P < 0.01$) (Fig. 6C, right panel). These results strongly suggest that the TRAIL pathway plays a major role in GBM cell survival. Then, we examined the protein level of TRAIL in the conditioned medium of UCB-MSCs and AT-MSCs by using ELISA. TRAIL protein in the culture medium was not detected both in UCB-MSCs and AT-MSCs (data not shown). Taken together, these results suggest that TRAIL expression in MSCs is important and may cause apoptosis efficiently as reported previously [35].

As CXCL12 was highly expressed in AT-MSCs compared to UCB-MSCs, we hypothesized that CXCL12 might act as a key antiapoptotic factor inhibiting the TRAIL pathway. ELISA analysis clearly revealed that AT-MSCs secreted ~11-fold increase of CXCL12 in the supernatant compared to UCB-MSCs (Supplementary Fig. S1E).

CXCL12 was added exogenously to GBM#1 culture with recombinant TRAIL, and the number of live and dead cells was scored. GBM#1 in the presence of TRAIL and CXCL12 showed a significantly increased number of live GBM#1 compared to TRAIL alone without CXCL12 on day 3 (with TRAIL: $0.8 \pm 0.2 \times 10^4$ cells; with TRAIL and CXCL12: $4.0 \pm 0.2 \times 10^4$ cells, $n = 3$, $P < 0.01$) and day 7 (with TRAIL: $2.6 \pm 0.1 \times 10^4$ cells; with TRAIL and CXCL12: $9.9 \pm 0.2 \times 10^4$ cells, $n = 3$, $P < 0.01$) (Fig. 6C, left panel). In addition, the number of GBM cells reached a level similar to that of GBM#1 alone or GBM#1 in the presence of TRAIL and CXCL12 on day 3 and day 7 (day 3: GBM alone: $3.4 \pm 0.2 \times 10^4$ cells, with TRAIL and CXCL12: $4.0 \pm 0.2 \times 10^4$ cells; day 7: GBM alone: $10 \pm 0.3 \times 10^4$ cells, with TRAIL and CXCL12: $9.9 \pm 0.2 \times 10^4$ cells, $n = 3$, $P < 0.01$) (Fig. 6C, left panel). Moreover, the number of dead GBM#1 cells decreased in the

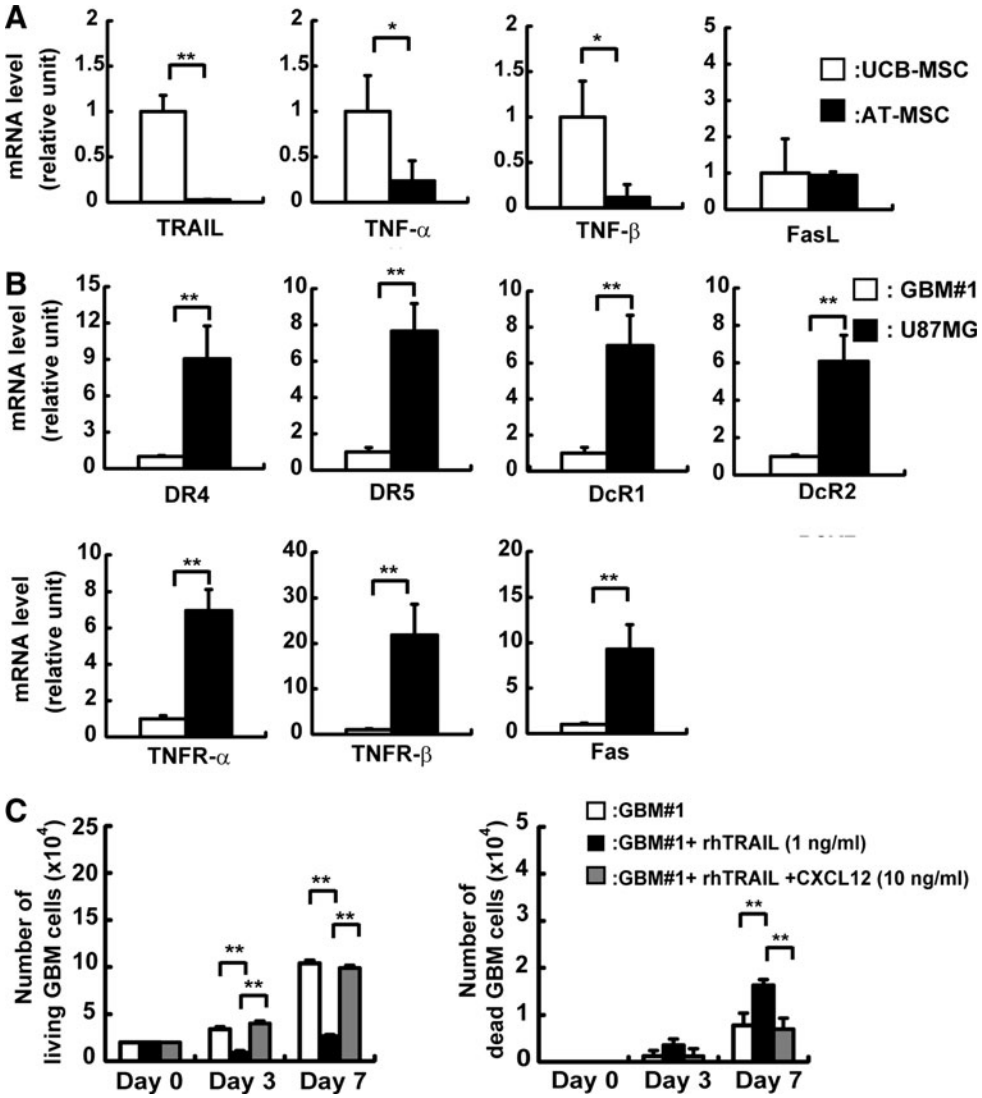


**FIG. 6.** Analysis of apoptosis derived from UCB-MSCs toward GBM#1. **(A)** mRNA expression of death ligands was analyzed in UCB-MSCs and AT-MSCs by real-time PCR. The expression of factors in UCB-MSCs was normalized to a value of 1 as the standard for each factor. *White bar*: UCB-MSCs; *black bar*: AT-MSCs (*$P < 0.05$; **$P < 0.01$). **(B)** mRNA expression of death receptors in GBM#1 and U87MG was analyzed by real-time PCR. The expression of factors in GBM#1 was normalized to a value of 1 as the standard for each receptor. *White bar*: GBM#1; *black bar*: U87MG (**$P < 0.01$). **(C)** The effect of tumor necrosis factor-related apoptosis-inducing ligand (TRAIL) and CXCL12 on GBM#1 survival was analyzed. The number of live GBM#1 was measured on days 3 and 7 in the presence of TRAIL (1 ng/mL) with or w/o CXCL12 (10 ng/mL) (*left graph*). The number of dead GBM#1 was measured in the presence of TRAIL (1 ng/mL) with or w/o CXCL12 (10 ng/mL) (*right graph*). *White bar*: GBM#1 alone; *black bar*; GBM#1 + recombinant TRAIL (1 ng/mL); *gray bar*; GBM#1 + recombinant TRAIL + recombinant CXCL12 (10 ng/mL). Note that GBM#1 death induced by TRAIL was inhibited in the presence of CXCL12.

presence of CXCL12 with TRAIL on day 7 compared to TRAIL alone (with TRAIL: $1.6 \pm 0.1 \times 10^4$ cells; with TRAIL and CXCL12: $0.7 \pm 0.2 \times 10^4$ cells, $n = 3$, $P < 0.01$) (Fig. 6C, right panel). These results indicate that CXCL12 plays a role inhibiting the TRAIL pathway in GBM development.

## Discussion

In this study, we analyzed the inhibitory effect of MSCs derived from different tissues on glioma cell proliferation. Because characteristics of established glioma cell lines vary in many aspects [30,33], we analyzed glioblastoma cells from patients representing a spectrum of primary brain tumors. Individual glioma cell lines secrete distinct kinds of growth factors and chemokines, suggesting that inhibitory effects of MSCs may vary depending on the glioma cell type. First, we isolated glioblastoma cells (GBM#1) and compared proliferation activity and mRNA expression of growth factor and chemokine to U87MG glioma cell lines (Fig. 1). As expected, U87MG proliferated faster than GBM#1 and expressed a higher level of mRNA of several kinds of growth factors and chemokines. Indeed, when U87MG and UCB-MSCs were cocultured at a higher ratio of 1:2, the number of U87MG did not decrease (Fig. 2B). Instead, the number of UCB-MSCs

significantly decreased, possibly because with exceptionally high proliferation activity of U87MG outcompeting UCB-MSCs. Similarly, when AT-MSCs were cocultured with U87MG for 7 days, the number of U87MG did not increase, but the number of AT-MSCs significantly decreased even when a high ratio of AT-MSCs was cocultured (Supplementary Fig. S1D). To characterize MSCs properly, primary brain tumor cells would be better to use in coculture assay, as they may more accurately reflect the in vivo effects on tumors in clinical applications.

Compared to BM-MSCs, UCB-MSCs have many advantages to use in cell-based therapy because of their relatively large ex vivo expansion capacity, low risk of viral infection, lack of donor morbidity, and less-pronounced immunogenicity [7,8,16]. In addition, the use of AT-MSCs has the advantages of large ex vivo expansion of capacity and less donor morbidity compared to the use of BM-MSCs. Because of the possibility of autotransplantation, the risk of immunorejection after transplantation of AT-MSCs is as low as after transplantation of BM-MSCs.

For most complete analysis of transplantation risk, it is important that precise and detailed analyses of characteristics of MSCs derived from different tissues should be performed, as well as analysis of MSCs after gene transduction for cell-based therapy. We found that among UCB-MSCs, AT-MSCs, and BM-MSCs, UCB-MSCs express the lowest level of CXCL12 (data not shown). Of note, the expression of TRAIL in UCB-MSCs promotes apoptosis of gliomas, and the effect of TRAIL toward gliomas is inhibited by CXCL12 (Fig. 6). This result suggests some parameters for selecting suitable MSCs for MSC-based cell therapy. CXCR4, the receptor for CXCL12, is known to be important in the migration, homing, and survival of several kinds of stem cells [36–38]. The roles of chemokines in tumor development, including glioma, have been studied through investigation of CXCL12 and its receptor CXCR4 [39–45]. The level of CXCL12 expression in glioma correlates well with the tumor grade, necrosis, angiogenesis, and invasiveness [46]. In fact, growth factors and those receptors expressed in glioma have been investigated in low-grade and high-grade gliomas, but expression of most of these are not precisely related to the tumor grade [47,48]. PDGF-α and PDGFR-α expression in glioma tends to relate to tumor grade due to an autocrine loop strongly associated with tumor progression [49].

Importantly, blockade of the CXCL12/CXCR4 axis in glioma cells inhibited glioma proliferation, invasion, and angiogenesis in vitro and in vivo. Recently a second receptor for CXCL12, CXCR7, has been identified [50,51]. CXCR7 is expressed in a number of cells, including EC [51,52], T cells [53], dendritic cells and B cells [54], chondrocytes [55], and endometrial stromal cells [56]. CXCR7 regulates cell adhesion and survival, but does not stimulate cell migration or mobilization of calcium ($Ca^{2+}$) [50]. Collectively, studies show that the CXCL12/CXCR4 axis mediates both chemotaxis and cell growth, whereas interaction of CXCR7 with CXCL12 promotes cell survival and cell growth [50,57]. Compared with U87MG, GBM#1 expressed a higher CXCR7 mRNA level and a lower CXCR4 mRNA level (Fig. 1E). CXCR7 shRNA experiments demonstrated that the CXCL12/CXCR7 axis might not be involved in cell growth of GBM#1. Transplantation of GBM#1 shCXCR7 showed no impairment of tumor growth or increase in number of apoptotic cells compared to control (Fig. 5). Unexpectedly, when GBM#1 shCXCR7 was cotransplanted with AT-MSCs, the number of apoptotic cells increased compared to the transplantation of shCXCR7 GBM#1 alone. However, the tumor weight did not significantly change compared with tumors derived from shCXCR7 GBM#1 alone. These results indicate that AT-MSCs can promote cell apoptosis when the CXCL12/CXCR7 pathway is inhibited in GBM. Further study is required to clarify the mechanism and to safely use AT-MSCs for cell-based therapy.

AT-MSCs express a higher level of mRNA of angiogenic factors, including PDGF, IGF, Ang-1, and VEGF than UCB-MSCs (Fig. 3). In fact, angiogenesis in tumors was accelerated when GBM#1 and AT-MSCs were cotransplanted in vivo (Fig. 4A, B). Therefore, PDGF-α and PDGFR-α act as an autocrine loop of glioma proliferation [49], suggesting that AT-MSCs would promote tumor progression of glioma as a paracrine loop via the PDGF-α/PDGFR-α axis (Fig. 1E).

In addition, the inhibition of the CXCL12/CXCR4 axis generates impairment of tumor-producing angiogenic factors, such as interleukin-8 and VEGF, resulting in the failure of tumor angiogenesis [58,59]. CXCL12 expression is crucial for tumor development associated with the tumor cell survival and tumor angiogenesis. Importantly, CXCL12 expression in tumors is highly associated with the prognosis of the patients [46,60]. Thus, MSCs must be carefully characterized with respect to CXCL12 production when applying MSC-based cell therapy to inhibit tumor cell proliferation.

While inoculation with UCB-MSCs reduced the size of GBM was observed in vivo, we did not achieve complete tumor regression (Fig. 4A). MSCs engineered to express TRAIL have been injected into glioma-bearing mice; results suggest that repeated administration of engineered UCB-MSCs might be necessary to consistently inhibit progressive GBM growth.

The proliferation of some cancer cells was enhanced by adding MSCs to the culture [27,28]. On the other hand, some groups have reported the anticancer activity of MSCs [14–22]. In fact, after BM-MSCs was transduced with therapeutic molecules [interferon-α (IFN-α), IFN-β, interleukin-12 (IL-12), IL-18, IL-23, IL-2, TRAIL, cytosine deaminase-uracil phosphoribosyl transferase (CD-UPRT), and thymidine kinase (TK)], anticancer activity was observed [14,17,19,22, 61,62]. In addition, AT-MSCs and UCB-MSCs were transduced with therapeutic molecules (CD-UPRT, TK, and TRAIL) and used for analysis of the mechanisms of inhibiting cancer cell proliferation [16,18,21,63,64]. Therefore, MSCs are used to investigate their roles of delivering targeting molecules, and characteristics of MSCs without transduction of targeting molecules have not been well studied. In agreement with previous reports suggesting contradictory effects of MSCs on tumor cell proliferation [16,65,66], we found that UCB-MSCs show tumor cell cytotoxicity, whereas AT-MSCs do not. The inhibitory effect of MSCs on other types of tumor proliferation should be investigated before MSCs are used as a tool for drug delivery.

In conclusion, for clinical application of MSCs, further investigation will be necessary to establish effective treatment strategies, with particular attention paid to the expression level of anticancer molecules in MSCs, appropriate time intervals of administration, and with extreme caution regarding expression of tumor-supporting factors.

## Acknowledgments

The authors thank Ms. Naomi Kaneko for excellent work on immunohistochemistry. This study was supported by a Grant-in-Aid for Scientific Research from the Japanese Ministry of Education, Culture, Sports, Science, and Technology.

## Author Disclosure Statement

No competing financial interests exist.

## References

1. Pittenger MF, AM Mackay, SC Beck, RK Jaiswal, R Douglas, JD Mosca, MA Moorman, DW Simonetti, S Craig and DR Marshak. (1999). Multilineage potential of adult human mesenchymal stem cells. Science 284:143–147.
2. Kern S, H Eichler, J Stoeve, H Kluter and K Bieback. (2006). Comparative analysis of mesenchymal stem cells from bone marrow, umbilical cord blood, or adipose tissue. Stem Cells 24:1294–1301.
3. Zuk PA, M Zhu, H Mizuno, J Huang, JW Futrell, AJ Katz, P Benhaim, HP Lorenz and MH Hedrick. (2001). Multilineage cells from human adipose tissue: implications for cell-based therapies. Tissue Eng 7:211–228.
4. Asakura A, M Komaki and M Rudnicki. (2001). Muscle satellite cells are multipotential stem cells that exhibit myogenic, osteogenic, and adipogenic differentiation. Differentiation 68:245–253.
5. De Bari C, F Dell'Accio, P Tylzanowski and FP Luyten. (2001). Multipotent mesenchymal stem cells from adult human synovial membrane. Arthritis Rheum 44:1928–1942.
6. Gronthos S, M Mankani, J Brahim, PG Robey and S Shi. (2000). Postnatal human dental pulp stem cells (DPSCs) *in vitro* and *in vivo*. Proc Natl Acad Sci U S A 97:13625–13630.
7. Nagano M, K Kimura, T Yamashita, K Ohneda, D Nozawa, H Hamada, H Yoshikawa, N Ochiai and O Ohneda. (2010). Hypoxia responsive mesenchymal stem cells derived from human umbilical cord blood are effective for bone repair. Stem Cells Dev 19:1195–1210.
8. Bieback K, S Kern, H Kluter and H Eichler. (2004). Critical parameters for the isolation of mesenchymal stem cells from umbilical cord blood. Stem Cells 22:625–634.
9. Parolini O, F Alviano, GP Bagnara, G Bilic, HJ Buhring, M Evangelista, S Hennerbichler, B Liu, M Magatti, et al. (2008). Concise review: isolation and characterization of cells from human term placenta: outcome of the first international Workshop on Placenta Derived Stem Cells. Stem Cells 26:300–311.
10. Tran TC, K Kimura, M Nagano, T Yamashita, K Ohneda, H Sugimori, F Sato, Y Sakakibara, H Hamada, et al. (2011). Identification of human placenta-derived mesenchymal stem cells involved in re-endothelialization. J Cell Physiol 226:224–235.
11. De Coppi P, G Bartsch, Jr., MM Siddiqui, T Xu, CC Santos, L Perin, G Mostoslavsky, AC Serre, EY Snyder, et al. (2007). Isolation of amniotic stem cell lines with potential for therapy. Nat Biotechnol 25:100–106.
12. Ciavarella S, F Dammacco, M De Matteo, G Loverro and F Silvestris. (2009). Umbilical cord mesenchymal stem cells: role of regulatory genes in their differentiation to osteoblasts. Stem Cells Dev 18:1211–1220.
13. Dominici M, K Le Blanc, I Mueller, I Slaper-Cortenbach, F Marini, D Krause, R Deans, A Keating, D Prockop and E Horwitz. (2006). Minimal criteria for defining multipotent mesenchymal stromal cells. The International Society for Cellular Therapy position statement. Cytotherapy 8:315–317.
14. Studeny M, FC Marini, RE Champlin, C Zompetta, IJ Fidler and M Andreeff. (2002). Bone marrow-derived mesenchymal stem cells as vehicles for interferon-beta delivery into tumors. Cancer Res 62:3603–3608.
15. Studeny M, FC Marini, JL Dembinski, C Zompetta, M Cabreira-Hansen, BN Bekele, RE Champlin and M Andreeff. (2004). Mesenchymal stem cells: potential precursors for tumor stroma and targeted-delivery vehicles for anticancer agents. J Natl Cancer Inst 96:1593–1603.
16. Ciavarella S, M Dominici, F Dammacco and F Silvestris. (2011). Mesenchymal stem cells: a new promise in anticancer therapy. Stem Cells Dev 20:1–10.
17. Nakamizo A, F Marini, T Amano, A Khan, M Studeny, J Gumin, J Chen, S Hentschel, G Vecil, et al. (2005). Human bone marrow-derived mesenchymal stem cells in the treatment of gliomas. Cancer Res 65:3307–3318.
18. Kang SG, SS Jeun, JY Lim, SM Kim, YS Yang, WI Oh, PW Huh and CK Park. (2008). Cytotoxicity of human umbilical cord blood-derived mesenchymal stem cells against human malignant glioma cells. Childs Nerv Syst 24:293–302.
19. Hong X, C Miller, S Savant-Bhonsale and SN Kalkanis. (2009). Antitumor treatment using interleukin-12-secreting marrow stromal cells in an invasive glioma model. Neurosurgery 64:1139–1147.
20. Hamada H, M Kobune, K Nakamura, Y Kawano, K Kato, O Honmou, K Houkin, T Matsunaga and Y Niitsu. (2005). Mesenchymal stem cells (MSC) as therapeutic cytoreagents for gene therapy. Cancer Sci 96:149–156.
21. Kim SM, JY Lim, SI Park, CH Jeong, JH Oh, M Jeong, W Oh, SH Park, YC Sung and SS Jeun. (2008). Gene therapy using TRAIL-secreting human umbilical cord blood-derived mesenchymal stem cells against intracranial glioma. Cancer Res 68:9614–9623.
22. Menon LG, K Kelly, HW Yang, SK Kim, PM Black and RS Carroll. (2009). Human bone marrow-derived mesenchymal stromal cells expressing S-TRAIL as a cellular delivery vehicle for human glioma therapy. Stem Cells 27:2320–2330.
23. Stupp R, WP Mason, MJ van den Bent, M Weller, B Fisher, MJ Taphoorn, K Belanger, AA Brandes, C Marosi, et al.; European Organisation for Research and Treatment of Cancer Brain Tumor and Radiotherapy Groups; National Cancer Institute of Canada Clinical Trials Group. (2005). Radiotherapy plus concomitant and adjuvant temozolomide for glioblastoma. N Engl J Med 352:987–996.
24. De Vleeschouwer S, F Van Calenbergh, P Demaerel, P Flamen, S Rutkowski, E Kaempgen, JE Wolff, C Plets, R Sciot and SW Van Gool. (2004). Transient local response and persistent tumor control in a child with recurrent malignant glioma: treatment with combination therapy including dendritic cell therapy. Case report. J Neurosurg 100:492–497.
25. Zhao D, J Najbauer, E Garcia, MZ Metz, M Gutova, CA Glackin, SU Kim and KS Aboody. (2008). Neural stem cell tropism to glioma: critical role of tumor hypoxia. Mol Cancer Res 6:1819–1829.
26. Ahmed AU, MA Tyler, B Thaci, NG Alexiades, Y Han, IV Ulasov and MS Lesniak. (2011). A comparative study of neural and mesenchymal stem cell-based carriers for oncolytic adenovirus in a model of malignant glioma. Mol Pharmacol 8:1559–1572.
27. Zhu W, W Xu, R Jiang, H Qian, M Chen, J Hu, W Cao, C Han and Y Chen. (2006). Mesenchymal stem cells derived from bone marrow favor tumor cell growth *in vivo*. Exp Mol Pathol 80:267–274.

28. Yu JM, ES Jun, YC Bae and JS Jung. (2008). Mesenchymal stem cells derived from human adipose tissues favor tumor cell growth *in vivo*. Stem Cells Dev 17:463–473.
29. Valter MM, OD Wiestler and T Pietsche. (1999). Differential control of VEGF synthesis and secretion in human glioma cells by IL-1 and EGF. Int J Dev Neurosci 17:565–577.
30. Hao C, IF Parney, WH Roa, J Turner, KC Petruk and DA Ramsay. (2002). Cytokine and cytokine receptor mRNA expression in human glioblastomas: evidence of Th1, Th2 and Th3 cytokine dysregulation. Acta Neuropathol 103:171–178.
31. Louis DN, H Ohgaki, OD Wiestler, WK Cavenee, PC Burger, A Jouvet, BW Scheithauer and P Kleihues. (2007). The 2007 WHO classification of tumours of the central nervous system. Acta Neuropathol 114:97–109.
32. Nagano M, T Yamashita, H Hamada, K Ohneda, K Kimura, T Nakagawa, M Shibuya, H Yoshikawa and O Ohneda. (2007). Identification of functional endothelial progenitor cells suitable for the treatment of ischemic tissue using human umbilical cord blood. Blood 110:151–160.
33. Folkerth RD. (2004). Histologic measures of angiogenesis in human primary brain tumors. Cancer Treat Res 117:79–95.
34. Hattermann K, J Held-Feindt, R Lucius, SS Muerkoster, ME Penfold, TJ Schall and R Mentlein. (2010). The chemokine receptor CXCR7 is highly expressed in human glioma cells and mediates antiapoptotic effects. Cancer Res 70:3299–3308.
35. Yang B, X Wu, Y Mao, W Bao, L Gao, P Zhou, R Xie, L Zhou and J Zhu. (2009). Dual-targeted antitumor effects against brainstem glioma by intravenous delivery. Neurosurgery 65:610–624.
36. Abbott JD, Y Huang, D Liu, R Hickey, DS Krause and FJ Giordano. (2004). Stromal cell-derived factor-1alpha plays a critical role in stem cell recruitment to the heart after myocardial infarction but is not sufficient to induce homing in the absence of injury. Circulation 110:3300–3305.
37. Mohle R, F Bautz, S Rafii, MA Moore, W Brugger and L Kanz. (1998). The chemokine receptor CXCR-4 is expressed on CD34+ hematopoietic progenitors and leukemic cells and mediates transendothelial migration induced by stromal cell-derived factor-1. Blood 91:4523–4530.
38. Son BR, LA Marquez-Curtis, M Kucia, M Wysoczynski, AR Turner, J Ratajczak, MZ Ratajczak and A Janowska-Wieczorek. (2006). Migration of bone marrow and cord blood mesenchymal stem cells *in vitro* is regulated by stromal-derived factor-1-CXCR4 and hepatocyte growth factor-c-met axes and involves matrix metalloproteinases. Stem Cells 24:1254–1264.
39. Bajetto A, F Barbieri, A Dorcaratto, S Barbero, A Daga, C Porcile, JL Ravetti, G Zona, R Spaziante, et al. (2006). Expression of CXC chemokine receptors 1–5 and their ligands in human glioma tissues: role of CXCR4 and SDF1 in glioma cell proliferation and migration. Neurochem Int 49:423–432.
40. Dewan MZ, S Ahmed, Y Iwasaki, K Ohba, M Toi and N Yamamoto. (2006). Stromal cell-derived factor-1 and CXCR4 receptor interaction in tumor growth and metastasis of breast cancer. Biomed Pharmacother 60:273–276.
41. Holland JD, M Kochetkova, C Akekawatchai, M Dottore, A Lopez and SR McColl. (2006). Differential functional activation of chemokine receptor CXCR4 is mediated by G proteins in breast cancer cells. Cancer Res 66:4117–4124.
42. Hong X, F Jiang, SN Kalkanis, ZG Zhang, XP Zhang, AC DeCarvalho, M Katakowski, K Bobbitt, T Mikkelsen and M Chopp. (2006). SDF-1 and CXCR4 are up-regulated by VEGF and contribute to glioma cell invasion. Cancer Lett 236:39–45.
43. Ma M, JY Ye, R Deng, CM Dee and GC Chan. (2011). Mesenchymal stromal cells may enhance metastasis of neuroblastoma via SDF-1/CXCR4 and SDF-1/CXCR7 signaling. Cancer Lett 312:1–10.
44. Park SA, CH Ryu, SM Kim, JY Lim, SI Park, CH Jeong, JA Jun, JH Oh, SH Park, W Oh and SS Jeun. (2011). CXCR4-transfected human umbilical cord blood-derived mesenchymal stem cells exhibit enhanced migratory capacity toward gliomas. Int J Oncol 38:97–103.
45. Sun X, G Cheng, M Hao, J Zheng, X Zhou, J Zhang, RS Taichman, KJ Pienta and J Wang. (2010). CXCL12/CXCR4/CXCR7 chemokine axis and cancer progression. Cancer Metastasis Rev 29:709–722.
46. Rempel SA, S Dudas, S Ge and JA Gutierrez. (2000). Identification and localization of the cytokine SDF1 and its receptor, CXC chemokine receptor 4, to regions of necrosis and angiogenesis in human glioblastoma. Clin Cancer Res 6: 102–111.
47. Salmaggi A, M Gelati, B Pollo, C Marras, A Silvani, MR Balestrini, M Eoli, L Fariselli, G Broggi and A Boiardi. (2005). CXCL12 expression is predictive of a shorter time to tumor progression in low-grade glioma: a single-institution study in 50 patients. J Neurooncol 74:287–293.
48. Yamanaka R, R Tanaka, T Saitoh and S Okoshi. (1994). Cytokine gene expression on glioma cell lines and specimens. J Neurooncol 21:243–247.
49. Hermanson M, K Funa, M Hartman, L Claesson-Welsh, CH Heldin, B Westermark and M Nister. (1992). Platelet-derived growth factor and its receptors in human glioma tissue. Cancer Res 52:3213–3219.
50. Burns JM, BC Summers, Y Wang, A Melikian, R Berahovich, Z Miao, ME Penfold, MJ Sunshine, DR Littman, et al. (2006). A novel chemokine receptor for SDF-1 and I-TAC involved in cell survival, cell adhesion, and tumor development. J Exp Med 203:2201–2213.
51. Miao Z, KE Luker, BC Summers, R Berahovich, MS Bhojani, A Rehemtulla, CG Kleer, JJ Essner, A Nasevicius, et al. (2007). CXCR7 (RDC1) promotes breast and lung tumor growth *in vivo* and is expressed on tumor-associated vasculature. Proc Natl Acad Sci U S A 104:15735–15740.
52. Raggo C, R Ruhl, S McAllister, H Koon, BJ Dezube, K Fruh and AV Moses. (2005). Novel cellular genes essential for transformation of endothelial cells by Kaposi's sarcoma-associated herpesvirus. Cancer Res 65:5084–5095.
53. Balabanian K, B Lagane, S Infantino, KY Chow, J Harriague, B Moepps, F Arenzana-Seisdedos, M Thelen and F Bachelerie. (2005). The chemokine SDF-1/CXCL12 binds to and signals through the orphan receptor RDC1 in T lymphocytes. J Biol Chem 280:35760–35766.
54. Infantino S, B Moepps and M Thelen. (2006). Expression and regulation of the orphan receptor RDC1 and its putative ligand in human dendritic and B cells. J Immunol 176:2197–2207.
55. Jones SW, SM Brockbank, ML Mobbs, NJ Le Good, S Soma-Haddrick, AJ Heuze, CJ Langham, D Timms, P Newham and MR Needham. (2006). The orphan G-protein coupled receptor RDC1: evidence for a role in chondrocyte hypertrophy and articular cartilage matrix turnover. Osteoarthritis Cartilage 14:597–608.
56. Okada H, T Nakajima, T Yoshimura, K Yasuda and H Kanzaki. (2003). Microarray analysis of genes controlled by progesterone in human endometrial stromal cells *in vitro*. Gynecol Endocrinol 17:271–280.
57. Wang J, Y Shiozawa, Y Wang, Y Jung, KJ Pienta, R Mehra, R Loberg and RS Taichman. (2008). The role of CXCR7/RDC1 as a chemokine receptor for CXCL12/SDF-1 in prostate cancer. J Biol Chem 283:4283–4294.

58. Salvucci O, L Yao, S Villalba, A Sajewicz, S Pittaluga and G Tosato. (2002). Regulation of endothelial cell branching morphogenesis by endogenous chemokine stromal-derived factor-1. Blood 99:2703–2711.
59. Ping YF, XH Yao, JH Chen, H Liu, DL Chen, XD Zhou, JM Wang and XW Bian. (2007). The anti-cancer compound Nordy inhibits CXCR4-mediated production of IL-8 and VEGF by malignant human glioma cells. J Neurooncol 84:21–29.
60. Zhou Y, PH Larsen, C Hao and VW Yong. (2002). CXCR4 is a major chemokine receptor on glioma cells and mediates their survival. J Biol Chem 277:49481–49487.
61. Aboody KS, J Najbauer and MK Danks. (2008). Stem and progenitor cell-mediated tumor selective gene therapy. Gene Ther 15:739–752.
62. Sasportas LS, R Kasmieh, H Wakimoto, S Hingtgen, JA van de Water, G Mohapatra, JL Figueiredo, RL Martuza, R Weissleder and K Shah. (2009). Assessment of therapeutic efficacy and fate of engineered human mesenchymal stem cells for cancer therapy. Proc Natl Acad Sci U S A 106:4822–4827.
63. Cavarretta IT, V Altanerova, M Matuskova, L Kucerova, Z Culig and C Altaner. (2010). Adipose tissue-derived mesenchymal stem cells expressing prodrug-converting enzyme inhibit human prostate tumor growth. Mol Ther 18:223–231.
64. Kucerova L, V Altanerova, M Matuskova, S Tyciakova and C Altaner. (2007). Adipose tissue-derived human mesenchymal stem cells mediated prodrug cancer gene therapy. Cancer Res 67:6304–6313.
65. Nakamura K, Y Ito, Y Kawano, K Kurozumi, M Kobune, H Tsuda, A Bizen, O Honmou, Y Niitsu and H Hamada. (2004). Antitumor effect of genetically engineered mesenchymal stem cells in a rat glioma model. Gene Ther 11:1155–1164.
66. Uchibori R, T Okada, T Ito, M Urabe, H Mizukami, A Kume and K Ozawa. (2009). Retroviral vector-producing mesenchymal stem cells for targeted suicide cancer gene therapy. J Gene Med 11:373–381.

Address correspondence to:
*Osamu Ohneda, MD, PhD*
*Department of Regenerative Medicine*
*University of Tsukuba*
*1-1-1 Tennodai*
*Tsukuba 305-8575*
*Japan*

*E-mail:* oohneda@md.tsukuba.ac.jp

Received for publication September 6, 2012
Accepted after revision December 10, 2012
Prepublished on Liebert Instant Online December 11, 2012